2020 International Conference on Unmanned Aircraft Systems (ICUAS)
Athens, Greece. September 1-4, 2020

Effects of Unsteady Aerodynamics on Gliding Stability of a Bio-Inspired UAV

Ernesto Sanchez-Laulhe[1], Ramon Fernandez-Feria[2], José Ángel Acosta[1], and Anibal Ollero[1]

Abstract— **This paper presents a longitudinal dynamic model to be used in the control of new animal flight bio-inspired UAVs designed to achieve better performance in terms of energy consumption, flight endurance, and safety when comparing with conventional multi-rotors. In order to control these UAVs, simple models are needed to predict its dynamics in real time by the on-board autopilots, which are very limited in term of computational resources. To that end, the model presented considers transitional aerodynamic unsteady effects, which change significantly the evolution of the system. The physical relevance of these aerodynamic unsteady terms in gliding flight is validated by comparing with results when these new terms are neglected. Finally, an analysis of dynamic stability is proposed in order to characterize the transitional phases of gliding flight.**

I. INTRODUCTION

Increasing flight endurance and the safety in the interaction with humans and objects in the environment are two very important topics in the evolution of small unmanned aerial systems. Bio-inspiration can play an important role to deal with these topics. Particularly, animal flight has been studied in order to being able of increasing the efficiency [1]-[3]. In fact, flight mechanics of birds and insects are the product of an evolution process which have improved their techniques into the most efficient ways of air travelling. Birds are able to travel long distances without need of flapping their wings. They just reach certain velocity and height, and then begin to descend at a very low angle, maximizing the lift to drag ratio [4], [5].

The idea is not new. For instance, [6] analyse the applications of insect flight aerodynamics for the design of micro UAVs. However, insect-inspired approach does not solve the autonomy problem for travelling long distances, for which bird-based approach has more sense. Several works have studied this kind of ornithopter, such as [7], and those reviewed in [8], in addition to other tailless articulated wings aircrafts [9], [10]. However, one of the main conclusions of the present work is the relevance of a well designed tail to control gliding.

In order to minimize energy consumption, optimizing gliding gets a huge importance. As aforementioned, the ability of travelling long distances with a minimal energetic requirement is one of the key point for the interest on bio-inspired vehicles. In this sense, there are several studies of the different flying behaviour of birds as a result of their wing characteristics. In [11] and [12] it is possible to find an exhaustive analysis of the differences between wings of sea birds, which have evolved in order to being able to fly long distances, and wings of birds of prey, which are ready to make more aggressive manoeuvres. Other works, as [13] and [14], focus on the lift generation from the aerodynamic surfaces during gliding.

In addition to the design characteristics, it is important to provide simple models in order to autonomously control the flight of the UAV with minimal computational resources as it is usually the case of the ornithopters. Numerical solutions of the Navier-Stokes equations have been used [15], but it is too expensive computationally for implementing it in real-time. For that reason, analytical models which work in a wide range of states result of much interest [16]. Other works are focused in operations with a deep stall to perform perching, as in [17],[18], although these models are defined for fixed wing gliders more similar to conventional aircrafts. In this sense, previous work in the present project [19] provided a simple solution for the longitudinal steady gliding of a bio-inspired UAV.

The contribution of this paper is to complement this work by means of a study of the longitudinal stability of the ornithopter gliding. In this sense, there are several works about animal flight stability. [20] analyses the static stability of birds from an aerodynamic point of view over a wide range of species, reaching relevant conclusions, such that flying a dihedral angle, even if it reduces the aerodynamic performance of the wing, helps to provide both longitudinal and lateral stability. This study also shows that tail is not always necessary for birds in order to provide stability. However, the recent study [21] finds that, unlike aircrafts, birds can fly with an important lift contribution from the tail, that also contributes to reduce drag in gliding flight. But, in order to maintain stability, these techniques that birds apply cannot be implemented for ornithopters with the current state of technology. Other conclusion of [20] is the importance of the position of the centre of gravity, as it happens also in aircrafts.

For the case of UAV there are also some works of interest. For instance, [22] uses bifurcation methods in order to obtain the lateral-directional stability modes of a bird-inspired design. [23] obtains flapping stability of an ornithopter by a study of limit cycles. The approach of this work is different, as it focuses on the longitudinal gliding dynamic stability by the linearisation of the system. This technique, based on previous works on aircraft stability [24], is aimed to control

*This work was supported by the European Project GRIFFIN ERC Advanced Grant 2017, Action 788247.

[1]University of Seville, GRVC Robotics Lab. Camino de los Descubrimientos S/N 41092, Seville, Spain. esanchezlaulhe@us.es, jaar@us.es, aollero@us.es

[2]University of Malaga, Mecanica de Fluidos, Dr Ortiz Ramos S/N, 29071, Malaga, Spain. ramon.fernandez@uma.es

the UAV in order to get a steady state in gliding flight. But the method is updated here to allow also for more aggressive manoeuvres, as this implies operations out of the steady states.

The paper is organised as follows. Section II defines the model, including new terms in relation to [19] to better capturing the transitions to the steady state. The effect of these new transient terms are analysed in Section III, considering also the stability modes for both cases, by means of a linearisation of the equations. Finally, Section IV summarizes the main conclusions and points out some future lines of research.

II. MODEL

In this section, the gliding dynamics of a bio-inspired UAV is formulated. The model used considers two lifting surfaces and the body of the vehicle, and it is based on that of [19], but with some changes in the formulation.

A. Non-dimensional Newton-Euler equations

In order to develop the Newton-Euler equations, the hypothesis of rigid body have been used. The non-dimensional equations which describe the longitudinal UAV behaviour are given by

$$2\mathcal{M}\frac{dU_b}{dt} = -U_b^2(C_D + Li + \Lambda C_{Dt}) - \sin(\gamma) \tag{1}$$

$$2\mathcal{M}U_b\frac{d\gamma}{dt} = U_b\left(C_L + \Lambda C_{Lt}\right) - \frac{\cos(\gamma)}{U_b} \tag{2}$$

$$\begin{aligned}\frac{1}{\chi U_b^2}\frac{dq}{dt} &= C_L\cos(\alpha) + C_D\sin(\alpha) \\ &\quad + \mathcal{L}\Lambda[C_{Lt}\cos(\alpha) + C_{Dt}\sin(\alpha)] \\ &\quad - \mathcal{R}_{HL}[C_L\sin(\alpha) - C_D\cos(\alpha)]\end{aligned} \tag{3}$$

$$\frac{d\theta}{dt} = q \tag{4}$$

where U_b is the velocity magnitude, γ its angle with the Earth reference frame, q the angular velocity, θ the pitch angle and α the wing's angle of attack, which can be computed by the difference between the pitch angle and the trajectory angle: $\alpha = \theta - \gamma$ (see Fig. 1). Note that the mass forces are considered to be applied only in the centre of gravity of the vehicle. Note also that the formulation in the trajectory frame simplifies the force equations in relation to [19], as the lift terms appears only in (1) whereas all the drag terms are in (2). However, (3) is formulated in the body reference frame as it is related to the rotation of the vehicle with the inertial frame.

The aerodynamics forces appearing on the UAV, depicted in Fig. 1, act in the aerodynamics centres of wing and tail and in the centre of gravity. These forces appear in (1)-(4) as the aerodynamic coefficients C_L, C_D, C_{Lt} and C_{Dt}, while the drag produced by the body is represented by the Lighthill number $Li = \frac{S_b}{S}C_{Db}$. Note that subscript "t" refers to the tail, while wing's aerodynamic forces are written without subscripts.

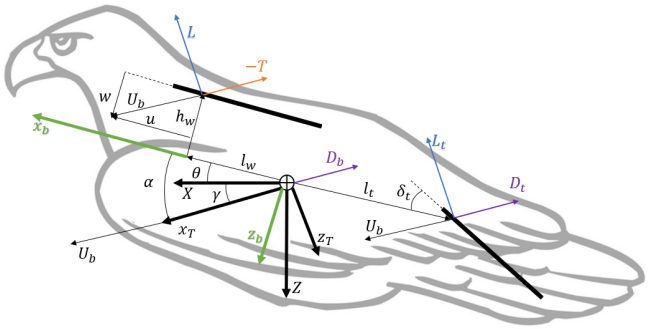

Fig. 1. Schematics of the ornithopter with the forces acting on it and all the reference frames of interest. Tail angle δ_t is the only control variable in the present work. x_b, z_b denote the body reference frame, x_T, z_T the trajectory frame and X, Z the Earth frame

The characteristic magnitudes of the problem (velocity, length and time) are the following

$$U_c = \sqrt{\frac{2mg}{\rho S}}, \qquad L_c = \frac{c}{2}, \qquad t_c = \sqrt{\frac{\rho S c^2}{8mg}} \tag{5}$$

with g the gravity acceleration, m the ornithopter mass, ρ the air density, S the effective wing surface and c the mean wing chord length. With this scaling, the non-dimensional parameters involved in the problem and appearing in (1)-(4) are

$$\begin{aligned}\mathcal{M} &= \frac{2m}{\rho S c}, \qquad \chi = \frac{1}{8}\rho S c^2\frac{l_w}{I_y} \\ \Lambda &= \frac{S_t}{S}, \qquad \mathcal{L} = \frac{l_t}{l_w}, \qquad \mathcal{R}_{HL} = \frac{h_w}{l_w}\end{aligned} \tag{6}$$

where I_y is the moment of inertia while l_w, h_w and l_t are the relative distances from the aerodynamics centres of the wing and the tail to the centre of gravity,

$$l_w = x_{cg} - x_{ac,w},\ h_w = z_{cg} - z_{ac,w},\ l_t = x_{cg} - x_{ac,t} \tag{7}$$

The aerodynamic centre of the wing is considered to be significantly above the longitudinal reference axis. The reason for this consideration is that it is usual to fly with an important dihedral angle, as it helps to the lateral stability [20]. This is one of the main differences of the models for bio-inspired gliders with those of conventional aircrafts, which make inadequate to use traditional stability frame models for ornithopters, as projections of forces change considerably.

B. Aerodynamic models

The approximation of very thin airfoils (actually, rectangular flat plates for the wings) is used for the aerodynamic forces. Then, considering the linear potential theory, which is appropriated for the Reynolds number of the ornithopter flight ($\sim 6 \times 10^4$) [1], Prandtl's lifting line theory gives the lift coefficient of the wing [25]

$$C_L = 2\pi\alpha \frac{\mathcal{AR}}{\mathcal{AR}+2} \tag{8}$$

where $\mathcal{AR}$ denotes the aspect ratio. For the tail, due to the bio-inspired design, the expression of a delta wing is more suitable [26], [27]. In addition, there is the issue that the angle of attack which the tail sees is not the angle of attack of the vehicle, because of the interference caused by the wing [25]. This difference in the effective angle of the tail is modelled proportional to the wing lift coefficient [28], and, considering the formula of this coefficient, it can also be simplified as $\varepsilon = \varepsilon_\alpha \alpha$, being $\varepsilon_\alpha = 0.3$ in this case. Then, it is obtained a lift coefficient given by

$$C_{Lt} = \frac{\pi}{2}\left[\alpha\left(1-\varepsilon_\alpha\right)+\delta_t\right]\mathcal{AR}_t \tag{9}$$

with δ_t being the deflection of the tail and $\mathcal{AR}_t$ the aspect ratio of the tail. However, these formulas are only valid in the steady state. Whenever angular velocities appear, there are unsteady effects which produce additional aerodynamics forces. They can be modelled at the typical Reynolds numbers of the UAV by the linear potential theory of unsteady thin airfoils [25]. Neglecting the small terms associated to the second temporal derivatives and to the weak effects of the unsteady wakes of wings and tail, they can be written as

$$C_{Lus} = 2\pi\left(\frac{1.5\dot{\alpha}-\frac{2l_w}{c}q}{U_b}\right)\frac{\mathcal{AR}}{\mathcal{AR}+2} \tag{10}$$

$$C_{Ltus} = \frac{\pi}{2}\left(\frac{1.5\dot{\alpha}-\frac{2l_t}{c}q}{U_b}\right)\mathcal{AR}_t \tag{11}$$

where the dot denotes temporal derivative. The above coefficients are added to the ones in (8) and (9) in order to obtain the total forces. Unsteady aerodynamic does not affect the steady state, as these are only transitional effects, but it is fundamental in the evolution to that state, as they work as damping terms in the glider dynamics. The pitch term comes from the vertical displacement of the wing or tail produced by the rotation around the center of gravity with angular velocity q, whereas the angle of attack rate term is produced by the rotation of the velocity vector with respect to the wing or tail.

As discussed in [19], stall of the lifting surfaces may lead to unphysical results. For this reason, a procedure of saturating the lift coefficients has been followed, reducing also the effects of the unsteady terms when the saturation conditions are reached. As explained in [19], these limitations are established at relatives angles of attack of 15^o for the wing and 35^o for the tail.

Finally, induced drag is modelled from Prandtl's lifting line theory in the linear limit as

$$C_{Di} = \frac{C_{Ls}^2}{\pi\mathcal{AR}}, \qquad C_{Dit} = \frac{C_{Lts}^2}{\pi\mathcal{AR}_t} \tag{12}$$

where the subscript "s" means the steady part of these coefficients, defined in (8) and (9).

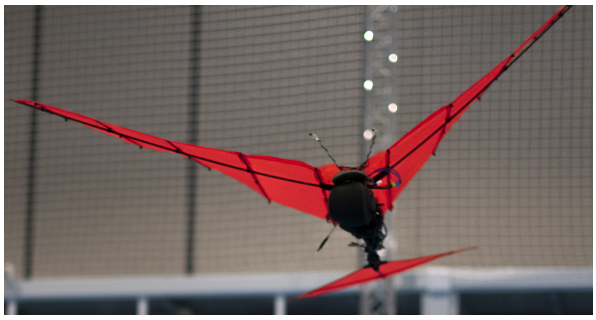

Fig. 2. Image of the reference prototype

III. Results and Discussion

In order to see the evolution of the variables during the transitional phase to the steady state, the ornithopter prototype showed in Fig. 2 has been used as reference. The aerodynamic surfaces of this UAV are made of fabric stiffened by carbon fiber ribs and spar, so aerodynamic theory used is reasonable as the wing can be considered as a rigid flat plate.

This vehicle has the capacity of alternating gliding and flapping modes but this paper is mainly focused on the gliding mode, as one of the great advantages of birds consists on their ability to travel long distances without flapping their wings. The values of the non-dimensional parameters for the prototype are written in Table I. All the results reported below are obtained with these values.

TABLE I
Magnitudes of the UAV

$\mathcal{M}$	Λ	$\mathcal{L}$	$\mathcal{R}_{HL}$	χ	Li	$\mathcal{AR}$	$\mathcal{AR}_t$
5.80	0.221	−9.60	1.12	0.133	0.005	4.78	2.35

The results analysed are focused on showing the effects of the unsteady aerodynamics on the gliding dynamics of the bio-inspired UAV. Firstly, the effect of these terms are analysed by comparing the evolution of the system of equations with and without them. Then, a stability analysis is proposed by means of the linearisation of the model, comparing the stability modes obtained.

A. Effect of unsteady aerodynamics

To better understand the effect that the unsteady aerodinamic coefficients (10)-(11) have on the vehicle's dynamics, the equations (1)-(4) have been solved numerically with and without these unsteady aerodynamic terms. The computation has been done by using the `ode45` function integrated in MATLAB (The MathWorks, Inc., Natick, MA, USA).

Table II shows the different sets of initial conditions used in the numerical simulations, all of them with the same control variable (tail angle δ_t), thus sharing the same gliding steady state (see [19]), which is also given in Table II. Note that dimensional variables are used in this section, with the same name as their dimensionless counterparts. Initial point

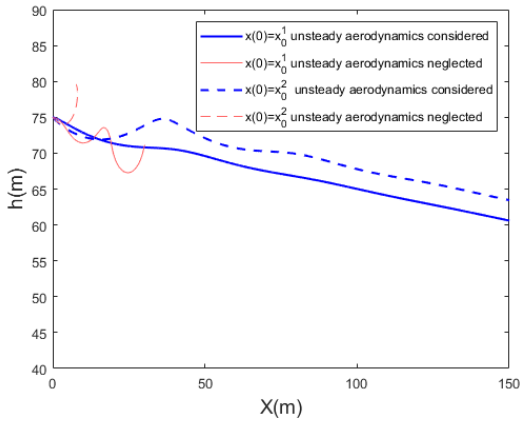

Fig. 3. Comparison between trajectories considering and neglecting unsteady aerodynamic, being X the longitudinal distance and h the height with respect to the Earth inertial frame.

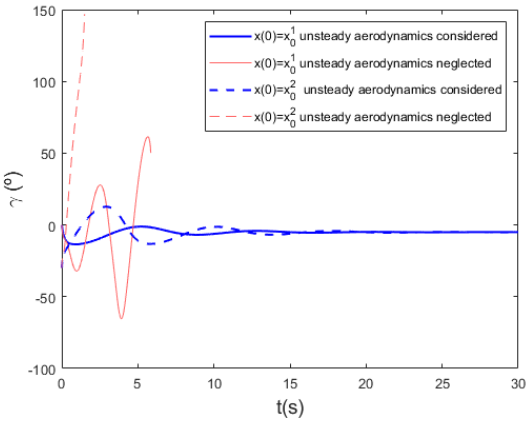

Fig. 4. Comparison between evolution of the trajectory angle considering and neglecting unsteady aerodynamic.

of the trajectory is defined at 0 in the longitudinal frame and a height of 75 m. Trajectories obtained with the first two sets of initial conditions are compared in Fig. 3, and results prove that oscillations in the trajectory of the system considering only steady aerodynamics are growing, until the computation is stopped as it reaches values where the model lose its applicability. However, the model considering unsteady coefficients reach the steady values.

TABLE II
DIMENSIONAL STATES

Initial conditions				
	$U_b(m/s)$	$\gamma(^o)$	q	$\theta(^o)$
$\mathbf{x_0^1}$	4.08	0	0	0
$\mathbf{x_0^2}$	12.23	-30	0	-20
$\mathbf{x_0^3}$	12.23	20	0	20
$\mathbf{x_0^4}$	4.08	0	0	10
$\mathbf{x_0^5}$	12.23	5	0	10
$\mathbf{x_0^6}$	8.15	0	0	-5
Steady state				
	$U_b(m/s)$	$\gamma(^o)$	q	$\theta(^o)$
$\mathbf{x_s}$	6.00	-5.02	0	0.40

The divergence of the system without considering the transient aerodynamic terms is clearer in the trajectory angle shown in Fig. 4 for the same initial conditions. The amplitude of the oscillations of the model without unsteady aerodynamic terms becomes very high even at the first peak, and then blows up after a few oscillations, while when the unsteady terms are taken into account low amplitude oscillations converge towards the steady state. A similar behaviour is observed for the speed (Fig. 5).

Figures 6 and 7 show the trajectory angle and the speed obtained considering the unsteady terms with all the different initial conditions given in Table II, thus showing that the ornithopter is capable of reaching the steady state for a wide range of initial conditions. The information in these two

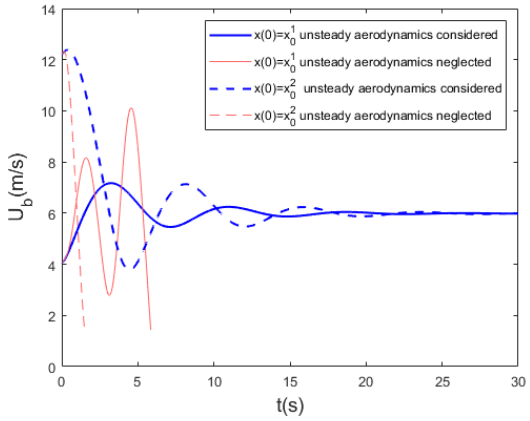

Fig. 5. Comparison between evolution of the velocity module considering and neglecting unsteady aerodynamic.

figures is plotted in Fig. 8 in a phase diagram, where it is clearly shown that these two variables, which are the most critical ones during the transient period, always converge to the to the steady state. In some cases, short period can also be observed as the first displacement in this diagram is not always following the spiral, for instance, with initial conditions 2 and 6.

B. Linearisation of the model

In order to numerically characterize the transition of the gliding until reaching the steady state, a linearisation of the model is proposed, with the objective of obtaining the stability modes. State variables are decomposed into a steady state and a perturbation:

$$U_b = U_{bs} + U_b(t) \tag{13}$$
$$\gamma = \gamma_s + \gamma(t) \tag{14}$$
$$q = q_s + q(t) \tag{15}$$
$$\theta = \theta_s + \theta(t) \tag{16}$$
$$\delta_t = \delta_{ts} + \delta_t(t) \tag{17}$$

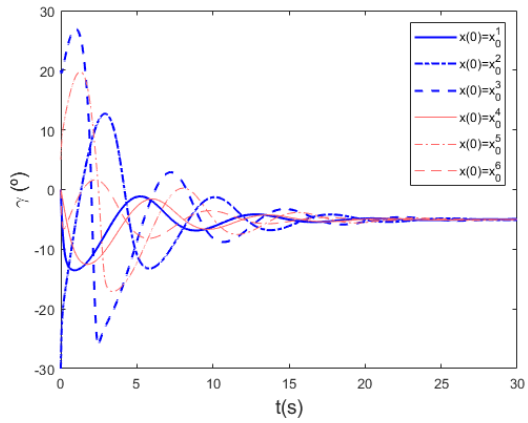

Fig. 6. Comparison of the evolution of the trajectory angle for different initial conditions.

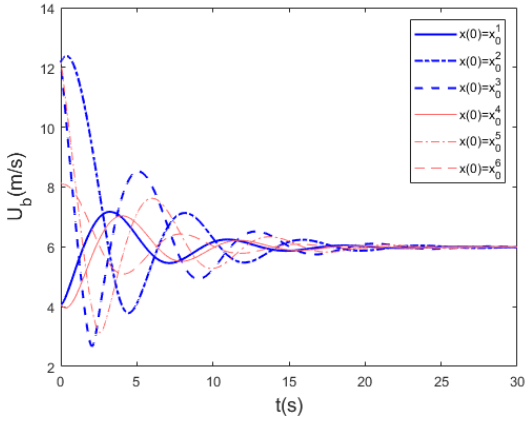

Fig. 7. Comparison of the evolution of the speed for different initial conditions.

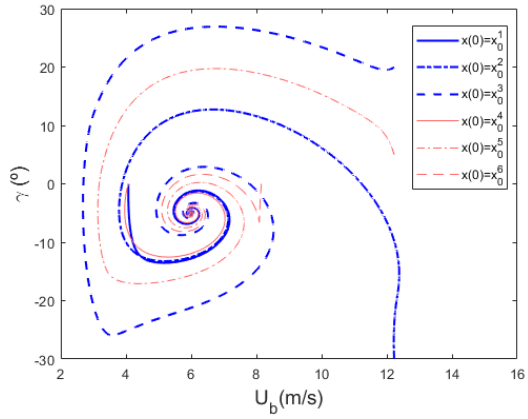

Fig. 8. Phase diagram for speed and trajectory angle with different initial conditions.

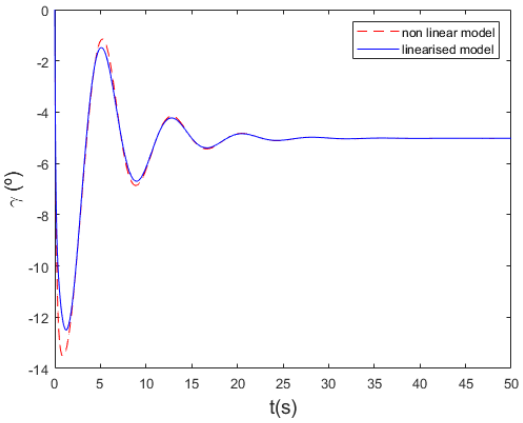

Fig. 9. Comparison between evolution of the trajectory angle given by the non-linear model and the linear approximation.

After substituting this decomposition into (1)-(4), they are linearised assuming small perturbations. Once the steady state terms are eliminated, the following descriptor (implicit) state-space model of linear equations is obtained for the perturbations:

$$M\begin{pmatrix}\dot{U}_b\\ \dot{\gamma}\\ \dot{q}\\ \dot{\theta}\end{pmatrix} = A\begin{pmatrix}U_b\\ \gamma\\ q\\ \theta\end{pmatrix} + B\delta_t \tag{18}$$

Note that we have selected the tail angle δ_t as the control parameter. Matrices M, A and B are given by

$$M = \begin{pmatrix} C_{X_{\dot{U}_b}} & 0 & 0 & 0\\ 0 & C_{Z_{\dot{\gamma}}} & 0 & C_{Z_{\dot{\theta}}}\\ 0 & C_{m_{\dot{\gamma}}} & C_{m_{\dot{q}}} & C_{m_{\dot{\theta}}}\\ 0 & 0 & 0 & 1 \end{pmatrix} \tag{19}$$

$$A = \begin{pmatrix} C_{X_{U_b}} & C_{X_\gamma} & 0 & C_{X_\theta}\\ C_{Z_{U_b}} & C_{Z_\gamma} & C_{Z_q} & C_{Z_\theta}\\ 0 & C_{m_\gamma} & C_{m_q} & C_{m_\theta}\\ 0 & 0 & 1 & 0 \end{pmatrix} \tag{20}$$

$$B = \begin{pmatrix} C_{X_{\delta_t}}\\ C_{Z_{\delta_t}}\\ C_{m_{\delta_t}}\\ 0 \end{pmatrix} \tag{21}$$

The coefficients depend of the equilibrium state chosen, which is obtained by the deflection of the tail. The definitions of each coefficient are formulated in Appendix I.

Figures 9 and Fig. 10 show the difference between the non-linear and linear models for the trajectory angle and speed, respectively. Results are quite similar, particularly in the damping of the system and the frequency of the response. Overshooting of both variables gives the highest error, which makes sense, because when the state is far from the linearisation point the approximation is less accurate.

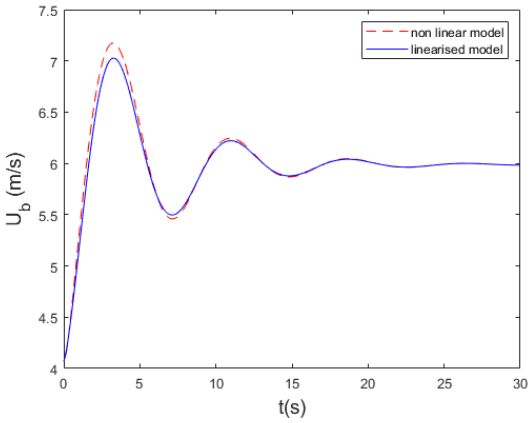

Fig. 10. Comparison between evolution of the velocity module given by the non-linear model and the linear approximation.

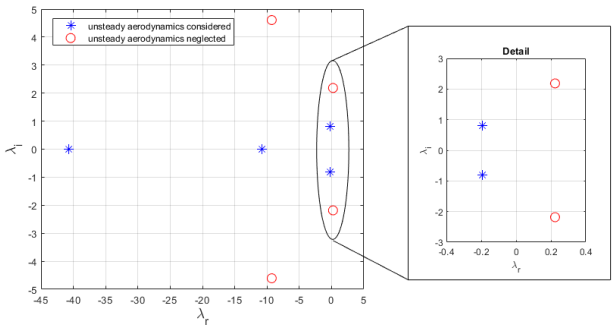

Fig. 11. Comparison between the eigenvalues $\lambda = \lambda_r + i\lambda_i$ in the complex plane obtained obtained with a without transient terms. The inset shows a zoom around the imaginary axis.

The effect of each variable are related to diverse physical effects. Velocity affects by means of the variation of the absolute aerodynamics forces. There is no velocity term in the third equation as all the terms in (3) are aerodynamic forces.

The angle of attack is represented in the variations of γ and θ, and it affects in two ways: variation of aerodynamic coefficients and change of projections of the forces. In fact, the static stability coefficient C_{m_α} is also in the equations as it is the same as C_{m_θ}. Coefficients of γ include also the change of the gravity force projections.

Unsteady aerodynamic is represented by the terms of q, $\dot{\gamma}$ and $\dot{\theta}$. Those coefficients are responsible of the damping of the system. $C_{X_{\dot{V}}}$ and $C_{Z_{\dot{\gamma}}}$ include the mass of the system, whereas $C_{m_{\dot{q}}}$ corresponds to the moment of inertia.

The control derivatives are related to the deflection of the tail, being the only control variable of the UAV of Fig. 2 in gliding mode. However, in the present gliding analysis, the effects of these terms is not going to be considered, as the focus here is on the free response of the glider, which is obtained just with the variables of the system. For the cases studied, the numerical values of the matrices are collected in the Appendix II. They correspond to the dimensionless parameters in Table I and for the steady state defined in Table II

C. Stability modes

The free-response of the solutions of the system (18) (without the forcing term δ_t), can be written as $\mathbf{x} = \mathbf{x_0}e^{\lambda t}$. Considering this solution, the different modes are obtained solving the generalised eigenvalue problem given by

$$|\mathbf{M}^{-1}\mathbf{A} - \lambda\mathbf{I}| = 0. \tag{22}$$

The eigenvalues and eigenvectors of the matrix $\mathbf{M}^{-1}\mathbf{A}$ characterize the dynamic stability of the glider. The eigenvalues λ, obtained numerically in MATLAB using the function `eig`, are plotted in the complex plane in Fig. 11. As expected, the system with the unsteady aerodynamic coefficients has all the eigenvalues with negative real part, whereas the simpler steady model has a pair of complex eigenvalues with positive real part, which causes the divergence of the transient dynamics. In Fig. 11 right these small values are clearer, as a zoom has been made near the imaginary axis.

The eigenvalues obtained when considering the unsteady aerodynamics are presented in Table III (to provide a more physical information, we give the dimensional values for the ornithopter with characteristics summarized in Table I):

TABLE III
EIGENVALUES OF THE SYSTEM

Unsteady aerodynamics considered		
λ_1	λ_2	$\lambda_{3,4}$
$-40.70\ s^{-1}$	$-10.76\ s^{-1}$	$-0.1943 \pm 0.8162i\ s^{-1}$
Unsteady aerodynamics neglected		
$\lambda_{1,2}$		$\lambda_{3,4}$
$-9.27 \pm 4.61\ s^{-1}$		$0.224 \pm 2.184\ s^{-1}$

TABLE IV
EIGENVECTORS OF THE SYSTEM

Unsteady aerodynamics considered			
	$\mathbf{x_{01}}$	$\mathbf{x_{02}}$	$\mathbf{x_{03,04}}$
U_{b_0}	-0.0289	0.0853	$0.9853_{\angle 0.9^o}$
γ_0	-0.1890	1	$0.3404_{\angle 86.1^o}$
q_0	1	0.0174	$0.0103_{\angle 1.3^o}$
θ_0	-0.5762	-0.0185	$0.3433_{\angle 104.7^o}$
Unsteady aerodynamics neglected			
	$\mathbf{x_{01,02}}$		$\mathbf{x_{03,04}}$
U_{b_0}	$0.1652_{\angle 140.5^o}$		$0.7629_{\angle 17.7^o}$
γ_0	$1_{\angle 180.0^o}$		$0.6930_{\angle 120.4^o}$
q_0	$0.1962_{\angle -1.5^o}$		$0.0573_{\angle 36.9^o}$
θ_0	$0.5288\angle 152.1^o$		$0.7286_{\angle 121.1^o}$

The eigenvectors associated to these modes are given in Table IV. From these values it is possible to compare the stability modes of the UAV as function of the unsteady aerodynamic terms:

- Fast modes: In the case of neglecting the unsteady aerodynamic, there is a single mode, an oscillatory convergence, mainly associated to angular variables. However, considering these terms, two exponential convergences appear, related to the angular acceleration and the trajectory angle. The dynamic is considerably fast with both models, as times to reduce to half amplitude with the updated model are of $0.0170\ s$ and $0.0644\ s$, similar to $0.0747\ s$ associated to the other system.
  These modes are related to the short period mode of an airplane, but their effects are different in both cases. When just the steady aerodynamic is considered, the angular pitch velocity seems not to be damped, when in aircraft is one of the most relevant of this mode. In the other case, due to the differences in the design between a regular fixed-wing aircraft and a bio-inspired vehicle, the short period is overdamped. It is relevant that the aerodynamic surfaces take almost all the plantform of the ornithopter which causes this overdamping of the mode.
  In Fig. 12, evolution of the trajectory angle shows the fast convergence of these modes. It also proves that the convergence is exponential, with a faster and a slower time.
- Slow modes: These are the modes which appear in Figures 4-10. Neglecting the unsteady aerodynamics, the mode is an oscillatory divergence, due to the lack of damping terms for the reacting moments of the glider. When these coefficients are considered, the mode changes becoming stable. Some reference values of the mode are written in Table V, where ω_n is the natural frequency, ξ the damping, $t_{1/2}$ the time to damp to half amplitude and t_2 the time to duplicate the perturbations. These characteristic values are clearly visible in Figures 4-10, particularly the frequencies and the times to damp or duplicate the perturbations.

TABLE V
CHARACTERISTIC VALUES OF PHUGOID MODE

Unsteady aerodynamics considered		
ω_n	ξ	$t_{1/2}$
$0.84\ rad/s$	0.232	$3.57\ s$
Unsteady aerodynamics neglected		
ω_n	ξ	t_2
$2.20\ rad/s$	-0.102	$3.10\ s$

This mode is similar to the phugoid of a conventional aircraft. From the eigenvectors associated, it is noticeable that trajectory angle and pitch angle have a very similar module and a small difference of phase, meaning that the variations on the angle of attack is significantly smaller than these other angles.
Fig. 13 shows the convergent oscillations of the trajectory angle in different phases. The characteristics seen in Table V are clearly visible. The phugoid is the main evolution seen in Figures 3-10.

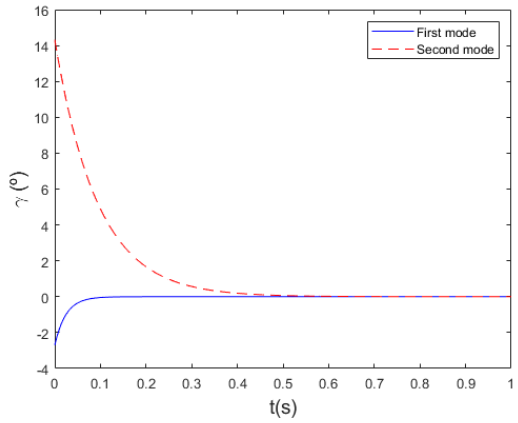

Fig. 12. Evolution of the trajectory angle for the fast modes.

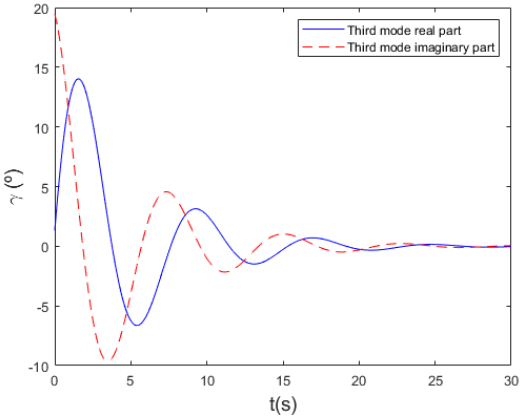

Fig. 13. Evolution of the trajectory angle for the slow modes.

IV. CONCLUSIONS

Due to the limitations of on-board instrumentation of bio-inspired systems, complex aerodynamic models or full aerodynamic simulations are impossible to implement for real-time control. These vehicles require of simpler analytical models as it had been stated in [19]. This study intends to complement this previous work by the extension of the validity of the model to unsteady cases.

In this sense, the results presented here shows that the dynamics of the model of [19] diverge before reaching the steady state, even when the system is statically stable. The update presented here, which includes unsteady aerodynamics coefficients, causes the system to converge to the steady state, taking values with much more physical meaning. It is worth mentioning that even if results for other prototypes may show convergence without the unsteady aerodynamics coefficients, neglecting them would affect trajectories obtained by simulations, showing a slower convergence.

The linearisation of the model around the steady state allows to obtain a numerical characterization of the dynamic stability of the system, in order to visualize the unsteady effects more clearly. By this process, results show that phugoid mode is unstable when unsteady aerodynamic effects are

neglected, but it became stable when they are considered. Results also show that the short period is overdamped, which makes sense considering that the relative size of the aerodynamics surfaces respect to the total vehicle size is more important than that of an aircraft. This characteristic also makes more relevant considering unsteady aerodynamics in bio-inspired UAVs.

The longitudinal model considered in this paper is quite more general, to our knowledge, than any other one considered before for modelling gliding ornithopters. Linearisation is also an important step towards an efficient control of the gliding flight, allowing to reach and maintain a certain angle of trajectory and optimizing the distance traveled. In order to extend this work it would be appropriated to obtain experimental data and confirm that the stability modes obtained theoretically corresponds to the actual flight. In this line, the work could also be extended to characterize the stability of flapping phases in combined gliding and flapping flight. For that task it would be appropriated to use a simplification for the flapping state, in order to characterize all the phases of the flight.

APPENDIX I
LINEARISATION COEFFICIENTS

$$C_{X_{\dot{U}_b}} = 2\mathcal{M} \tag{23}$$

$$C_{m_{\dot{q}}} = \frac{1}{\chi} \tag{24}$$

$$C_{Z_{\dot{\gamma}}} = U_{bs}\left(2\mathcal{M} + 3\pi\frac{\mathit{A\!R}}{\mathit{A\!R}+2} + \Lambda 3\pi\frac{\mathit{A\!R}_t}{4}\right) \tag{25}$$

$$C_{m_{\dot{\gamma}}} = U_{bs}\left[\left(3\pi\frac{\mathit{A\!R}}{\mathit{A\!R}+2} + \mathcal{L}\Lambda 3\pi\frac{\mathit{A\!R}_t}{4}\right)\cos(\alpha_s) - \mathcal{R}_{HL}3\pi\frac{\mathit{A\!R}}{\mathit{A\!R}+2}\sin(\alpha_s)\right] \tag{26}$$

$$C_{Z_{\dot{\theta}}} = -U_{bs}\left(3\pi\frac{\mathit{A\!R}}{\mathit{A\!R}+2} + \Lambda 3\pi\frac{\mathit{A\!R}_t}{4}\right) \tag{27}$$

$$C_{m_{\dot{\theta}}} = -U_{bs}\left[\left(3\pi\frac{\mathit{A\!R}}{\mathit{A\!R}+2} + \mathcal{L}\Lambda 3\pi\frac{\mathit{A\!R}_t}{4}\right)\cos(\alpha_s) - \mathcal{R}_{HL}3\pi\frac{\mathit{A\!R}}{\mathit{A\!R}+2}\sin(\alpha_s)\right] \tag{28}$$

$$C_{X_{U_b}} = -2U_{bs}\left(C_{Ds} + Li + \Lambda C_{Dts}\right) \tag{29}$$

$$C_{Z_{U_b}} = 2U_{bs}\left(C_{Ls} + \Lambda C_{Lts}\right) \tag{30}$$

$$C_{Z_q} = U_{bs}\left(-\frac{2\pi\mathit{A\!R}}{\mathit{A\!R}+2}\frac{2l_w}{c} - \Lambda\pi\mathit{A\!R}_t\frac{l_t}{c}\right) \tag{31}$$

$$C_{m_q} = U_{bs}\left[\left(-\frac{2\pi\mathit{A\!R}}{\mathit{A\!R}+2}\frac{2l_w}{c} - \mathcal{L}\Lambda\pi\mathit{A\!R}_t\frac{l_t}{c}\right)\cos(\alpha_s) + \mathcal{R}_{HL}\frac{2\pi\mathit{A\!R}}{\mathit{A\!R}+2}\frac{2l_w}{c}\sin(\alpha_s)\right] \tag{32}$$

$$C_{X_\gamma} = U_{bs}^2\left[\frac{4C_{Ls}}{\mathit{A\!R}+2} + \Lambda C_{Lts}\left(1-\varepsilon_\alpha\right)\right] - \cos(\gamma_s) \tag{33}$$

$$C_{Z_\gamma} = -U_{bs}^2\left[\frac{2\pi\mathit{A\!R}}{\mathit{A\!R}+2} + \Lambda\frac{\pi\mathit{A\!R}_t}{2}\left(1-\varepsilon_\alpha\right)\right] + \sin(\gamma_s) \tag{34}$$

$$C_{m_\gamma} = U_{bs}^2\Bigg\{\left(C_{Ls} + \mathcal{L}\Lambda C_{Lts}\right)\sin(\alpha_s) - \left[\frac{2\pi\mathit{A\!R}}{\mathit{A\!R}+2} + \mathcal{L}\Lambda\frac{\pi\mathit{A\!R}_t}{2}\left(1-\varepsilon_\alpha\right)\right]\cos(\alpha_s) - \left[\frac{4C_{Ls}}{\mathit{A\!R}+2} + \mathcal{L}\Lambda C_{Lts}\left(1-\varepsilon_\alpha\right)\right]\sin(\alpha_s) - \left(C_{Ds} + \Lambda C_{Dts}\right)\cos(\alpha_s) + \mathcal{R}_{HL}\left[\frac{2\pi\mathit{A\!R}}{\mathit{A\!R}+2}\sin(\alpha_s) + C_{Ls}\cos(\alpha_s) - \frac{4C_{Ls}}{\mathit{A\!R}+2}\cos(\alpha_s) + C_{Ds}\sin(\alpha_s)\right]\Bigg\} \tag{35}$$

$$C_{X_\theta} = -U_{bs}^2\left[\frac{4C_{Ls}}{\mathit{A\!R}+2} + \Lambda C_{Lts}\left(1-\varepsilon_\alpha\right)\right] \tag{36}$$

$$C_{Z_\theta} = U_{bs}^2\left[\frac{2\pi\mathit{A\!R}}{\mathit{A\!R}+2} + \Lambda\frac{\pi\mathit{A\!R}_t}{2}\left(1-\varepsilon_\alpha\right)\right] \tag{37}$$

$$C_{m_\theta} = U_{bs}^2\Bigg\{-\left(C_{Ls} + \mathcal{L}\Lambda C_{Lts}\right)\sin(\alpha_s) + \left[\frac{2\pi\mathit{A\!R}}{\mathit{A\!R}+2} + \mathcal{L}\Lambda\frac{\pi\mathit{A\!R}_t}{2}\left(1-\varepsilon_\alpha\right)\right]\cos(\alpha_s) + \left[\frac{4C_{Ls}}{\mathit{A\!R}+2} + \mathcal{L}\Lambda C_{Lts}\left(1-\varepsilon_\alpha\right)\right]\sin(\alpha_s) + \left(C_{Ds} + \Lambda C_{Dts}\right)\cos(\alpha_s) - \mathcal{R}_{HL}\left[\frac{2\pi\mathit{A\!R}}{\mathit{A\!R}+2}\sin(\alpha_s) + C_{Ls}\cos(\alpha_s) - \frac{4C_{Ls}}{\mathit{A\!R}+2}\cos(\alpha_s) + C_{Ds}\sin(\alpha_s)\right]\Bigg\} \tag{38}$$

$$C_{X_{\delta_t}} = -\Lambda U_{bs}^2 C_{Lts} \tag{39}$$

$$C_{Z_{\delta_t}} = \Lambda U_{bs}^2\frac{\pi\mathit{A\!R}_t}{2} \tag{40}$$

$$C_{m_{\delta_t}} = \Lambda U_{bs}^2\mathcal{L}\left[\frac{\pi\mathit{A\!R}_t}{2}\cos(\alpha_s) + C_{Lts}\sin(\alpha_s)\right] \tag{41}$$

APPENDIX II
DESCRIPTOR STATE-SPACE MODEL

The numerical values of the used in the simulations of section III-C are the following

$$M = \begin{pmatrix} 11.61 & 0 & 0 & 0 \\ 0 & 28.62 & 0 & -11.56 \\ 0 & -8.46 & 30.07 & 8.46 \\ 0 & 0 & 0 & 1 \end{pmatrix} \tag{42}$$

$$A = \begin{pmatrix} -0.12 & -0.40 & 0 & -0.60 \\ 1.36 & -10.89 & 1.71 & 10.80 \\ 0 & 3.73 & -39.58 & -3.73 \\ 0 & 0 & 1 & 0 \end{pmatrix} \tag{43}$$

$$B = \begin{pmatrix} -0.09 \\ 1.76 \\ -16.90 \\ 0 \end{pmatrix} \tag{44}$$

REFERENCES

[1] C. J. Pennycuick, *Modelling the flying bird*, Elsevier, 2008.

[2] U. M. Norberg, *Vertebrate flight: mechanics, physiology, morphology, ecology and evolution*. Springer, 2012.

[3] R. Dudley, *The biomechanics of insect flight: form, function, evolution*. Princeton University Press, 2002.

[4] B. W. Tobalske, "Biomechanics of bird flight," *Journal of Experimental Biology*, vol. 210, no. 18, pp. 3135–3146, 2007.

[5] U. L. Norberg, "Flight and scaling of flyers in nature," *Flow Phenomena in Nature*, vol. 1, pp. 120–154, 2007.

[6] C. P. Ellington, "The novel aerodynamics of insect flight: applications to micro-air vehicles," *Journal of experimental biology*, vol. 202, no. 23, pp. 3439–3448, 1999.

[7] J. A. Grauer and J. E. Hubbard, "Multibody model of an ornithopter," *Journal of guidance, control, and dynamics*, vol. 32, no. 5, pp. 1675–1679, 2009.

[8] H. E. Taha, M. R. Hajj, and A. H. Nayfeh, "Flight Dynamics and Control of Flapping-Wing MAVs: A Review," *Nonlinear Dynamics*, vol. 70, pp. 907–939, 2012.

[9] Q.-V. Nguyen and W. L. Chan, "Development and flight performance of a biologically-inspired tailless flapping-wing micro air vehicle with wing stroke plane modulation," *Bioinspiration & biomimetics*, vol. 14, no. 1, p. 016015, 2018.

[10] A. Paranjape, S. J. Chung and M. S. Selig, "Flight mechanics of a tailless articulated wing aircraft," *Bioinspiration & Biomimetics,* vol. 6, no. 2, pp. 026005, 2011.

[11] C. Pennycuick, "Thermal soaring compared in three dissimilar tropical bird species, fregata magnificens, pelecanus occidentals and coragyps atratus," *Journal of Experimental Biology*, vol. 102, no. 1, pp. 307–325, 1983.

[12] C. Pennycuick, "Soaring behaviour and performance of some east african birds, observed from a motor-glider," *Ibis*, vol. 114, no. 2, pp. 178–218, 1972.

[13] P. Henningsson and A. Hedenström, "Aerodynamics of gliding flight in common swifts," *Journal of experimental biology*, vol. 214, no. 3, pp. 382-393, 2011.

[14] P. Henningsson, A. Hedenström and R. J. Bomphrey, "Efficiency of Lift Production in Flapping and Gliding Flight of Swifts," *PLOS ONE*, vol. 9, no. 2, pp. 1-7, 2014.

[15] A. Paranjape, M. R. Dorothy, S. J. Chung and K. D. Lee, "A flight mechanics-centric review of bird-scale flapping flight," *International journal of aeronautical and space science*, vol. 13, no. 3, pp. 267-282, 2012.

[16] J. S. Lee, J. K. Kim, D. K. Kim and J. H Han, "Longitudinal flight dynamics of bio-inspired ornithopter considering fluid-structure integration," *Journal of guidance, control and dynamics*, Vol. 34, no. 3, pp. 667-677, 2011.

[17] J. W. Roberts, R. Cory and R. Tedrake, "On the controllability of fixed-wing perching," 2009 American Control Conference, St. Louis, MO, pp. 2018-2023, 2009.

[18] R. Cory and R. Tedrake, "Experiments in Fixed-Wing UAV Perching," AIAA Guidance, Navigation and Control Conference and Exhibit, 2008

[19] A. Martin-Alcantara, P. Grau, R. Fernandez-Feria and A. Ollero, "A simple model for gliding and low-amplitude flapping flight of a bio-inspired UAV," *2019 International Conference on Unmanned AircraftSystems (ICUAS)*, pp. 729-737, 2019.

[20] A. Thomas and G. Taylor, "Animal flight dynamics I. longitudinal stability in gliding flight," *Journal of theoretical biology*, vol. 212, no. 3, pp. 399–424, 2001.

[21] J. R. Usherwood, J. A. Cheney, J. Song, S. P. Windsor, J. P. J. Stevenson, U. Dierksheide, A. Nila and R. J. Bomphrey, "High aerodynamic lift from the tail reduces drag in gliding raptors," *Journal of experimental biology*, vol. 223, no. 3, 2020.

[22] A. Paranjape, N. K. Sinha and N. Ananthkrishnan, "Use of bifurcation and continuation methods for aircraft trim and stability analysis - a state-of-the-art," *45th AIAA Aerospace Sciences Meeting and Exhibit*, 2007.

[23] J. M. Dietl and E. Garcia, "Stability in ornithopter longitudinal flight dynamics," *Journal of Guidance, Control, and Dynamics*, vol. 31, no. 4, pp. 1157–1163, 2008.

[24] D. McLean, *Automatic flight control systems*, Prentice Hall, 1990.

[25] J. Katz and A. Plotkin, *Low-Speed Aerodynamics*, Cambridge University Press, 2001.

[26] A. L. Thomas, "On the aerodynamics of birds' tails," *Philosophical Transactions of the Royal Society of London. Series B: Biological Sciences*, vol. 340, no. 1294, pp. 361–380, 1993.

[27] R. T. Jones, *Wing Theory*, Princeton University Press, 1990.

[28] A. Silverstein and S. Katzoff, "Design charts for predicting downwash angles and wake characteristics behind plain and flapped wings," NACA-Report No. 648, 1915.